

Subdiffraction resolution in total internal reflection fluorescence microscopy with a grating substrate

Anne Sentenac,* Kamal Belkebir, Hugues Giovannini, and Patrick C. Chaumet

Institut Fresnel (CNRS UMR 6133), Université d'Aix-Marseille I & III, Avenue Escadrille Normandie-Niemen, F-13397 Marseille Cedex 20, France

*Corresponding author: anne.sentenac@fresnel.fr

Received July 3, 2007; revised December 11, 2007; accepted December 13, 2007;
posted January 3, 2008 (Doc. ID 87952); published January 29, 2008

We propose a fluorescence surface imaging system that presents a power of resolution beyond that of the diffraction limit without resorting to saturation effects or probe scanning. This is achieved by depositing the sample on an optimized periodically nanostructured substrate in a standard total internal reflection fluorescence microscope. The grating generates a high-spatial-frequency light grid that can be moved throughout the sample by changing the incident angle. An appropriate reconstruction procedure permits one to recover the fluorescence amplitude from the images obtained for various incidences. Simulations of this imaging system show that the resolution is not limited by diffraction but by the period of the grating.

© 2008 Optical Society of America

OCIS codes: 110.0180, 050.2770, 240.6680.

Far-field optical microscopy remains the most widely used imaging tool in the biology domain because of its unique noninvasive properties and the ability of staining the components of interest with fluorescent markers. Unfortunately the resolution of this far-field imaging technique is fundamentally limited by the diffraction process, to roughly several hundreds of nanometers with visible incident light [1]. Hence, improving the spatial resolution of optical fluorescence microscopes has been a major challenge in the past 20 years. One breakthrough in high-resolution optical imaging has been obtained by taking advantage of nonlinear optical effects in the fluorescence process [2]. Various techniques based on this principle provide resolution of the order of a few tens of nanometers [2,3]. Yet this spectacular amelioration is achieved at the expense of a certain readiness of utilization and the need for special fluorescent markers to avoid the frequent occurrence of photobleaching [4]. The other active field of research in high-resolution optical microscopy is not dedicated to fluorescent samples but is restricted to surface imaging. In this case, the diffraction barrier is broken by detecting the nonpropagating high-frequency light waves generated by the object. In near-field optical microscopy, this is done by scanning a nanosized tip or a diffractive element [5] in the vicinity of the sample [6]. More recently, several groups have proposed to deposit the sample on nanostructured dielectric-metallic substrates that are able to out-couple the high-spatial-frequency evanescent diffracted waves into detectable propagating ones [7–9], or equivalently to provide an illumination presenting high spatial frequencies [10,11]. The main advantages of these promising new paths in high-resolution optical imaging are that they do not require any scanning of the sample and the difficulties of their experimental implementations lie essentially in the making of the substrate.

In this paper, we extend the recent concepts on grating-assisted imaging [10,11] to propose a surface-imaging tool of fluorescent samples with a resolution well beyond the diffraction barrier. Our approach is based on total internal reflection fluorescent microscopy (TIRFM), which is widely used in biological studies, especially for the observation of plasma membranes of cells or single biomolecular dynamics [12]. In this technique, the excitation field is an evanescent wave obtained by the total internal reflection of a light beam at the interface between high- and low-index semi-infinite media. This configuration is adapted to surface imaging inasmuch as only the fluorescent markers close to the interface are strongly illuminated. To enhance the transverse resolution of TIRFM, while keeping its wide-field operation, it has been proposed to illuminate the sample with a standing-wave pattern [13–15] obtained from the interference of two or four waves. The transverse resolution of standing wave-TIRFM (SW-TIRFM) has been shown to be twice as good as that of TIRFM, approximately 100 nm [16] for an illumination wavelength of 500 nm [16,17]. Basically, it is limited by the period of the excitation light grid that is always bigger than $\lambda/(2n)$, where n is the prism index of refraction. To avoid this limitation, we propose to develop a grating-assisted TIRFM (GA-TIRFM) in which the interference setup of SW-TIRFM is discarded and the sample is illuminated by a subdiffraction light grid generated through a periodically nanostructured substrate.

More precisely, the sample is deposited on a planar permittivity grating that is illuminated, under total internal reflection, through an immersed objective, as shown in Fig. 1. The fluorescence is collected with the same immersed objective as in the experimental mounting proposed by Chung *et al.* [16]. The grating is designed so that it generates a high-frequency light grid that changes when the azimuthal incident

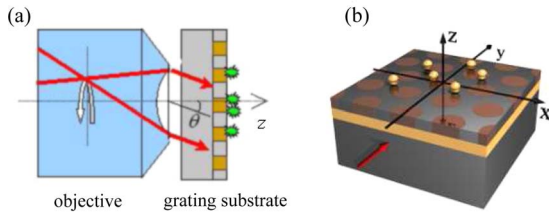


Fig. 1. (Color online) (a) Outline of the proposed experimental setup. The fluorescent sample is deposited on a grating that is illuminated by one plane wave in total internal reflection configuration through an immersed objective. The fluorescence is collected through the same objective, and its image is formed on the image plane of the microscope. A total of 24 images are recorded by successively illuminating the sample under different incidence. (b) Zoom of the grating substrate.

angle of the illumination beam is varied. The sample is illuminated with different angles of incidence, and an appropriate reconstruction scheme is used to build the map of fluorescence density from the images recorded by the microscope. An important feature of our system is that it does not require one to mount an interference setup in the microscope, as in SW-TIRFM. Hence, it can be implemented in a standard TIRFM system by replacing the sample support by a structured substrate.

The main issue of this imaging system lay in the design of the permittivity grating. Ideally, the field intensity in the close vicinity of the substrate should mimic, with a period smaller than $\lambda/2n$, that of the interference pattern of the SW-TIRFM. The intensity should be highly contrasted for each incidence and provide uniform illumination when averaged over all the incidences. Now, subwavelength gratings with high-permittivity contrast present a strongly modulated intensity pattern. But such a pattern has little dependence on the angle of incidence, as it is mainly due to the field jumps at the permittivity discontinuities. On the other hand, the intensity above a subwavelength grating with weak permittivity contrast is almost homogeneous. To avoid these two pitfalls, we have considered a grating with a moderate permittivity contrast that supports an electromagnetic eigenmode with high spatial frequency k_p at the incident wavelength λ [10]. In this case, the Fourier components of the transmitted pseudoperiodic field that correspond to spatial frequencies close to k_p are enhanced through the resonance phenomenon [18]. The interference between the zero-order and the resonant high-order field components yields a contrasted intensity pattern that is not linked spatially to the permittivity variations. In this work, we consider a 9 nm thin silver film, $n_{Ag} = 0.12 + 2i$ at $\lambda = 500$ nm, deposited on a glass substrate ($n_{sub} = 1.5$), that supports a high-frequency surface plasmon with wavenumber $k_p \approx 52\pi/\lambda$ [19]. The metallic film is covered by a 8 nm thin slab of resin, $n_{resin} = 1.5$, decorated by a hexagonal array of Ta_2O_5 rods with 80 nm diameter, $n_{Ta_2O_5} = 2$, and period $d = 120$ nm $\approx \lambda/4$. We illuminate the grating with an incident plane wave coming from the glass substrate that is p -polarized (electric field in the plane of incidence) with fixed polar angle of 70°

and various azimuthal angles ϕ . Simulations of the field just above the grating, performed with a rigorous coupled wave method [20], show that the periodic intensity pattern is strongly modulated, the ratio between the maxima and minima being close to 5, and that the hot and dark spot positions are significantly displaced when ϕ is varied. The illumination averaged over all the angles still presents a periodic modulation, but the ratio between the maxima and minima has been reduced to 1.7. All the field Fourier components decay exponentially, though with different rates, as one moves away from the interface. With our grating, the intensity maximum at $z = 5$ nm is ten times bigger than that at $z = 50$ nm. Note that in SW-TIRFM the intensity at $z = 5$ nm is, at best, two times bigger than that at $z = 50$ nm.

We now turn to the simulation of a GA-TIRFM experiment. The mathematical formulation of the image formation is given by [13,15]

$$I_l(\mathbf{r}) = [(O \times E_l) \otimes P](\mathbf{r}) + B, \quad \text{for } l = 1, \dots, N, \quad (1)$$

where O is the fluorophore density, P is the point spread function of the microscope, I_l is the l th recorded intensity on the image plane of the microscope, and E_l is the field intensity above the grating for the l th incident angle. The data are corrupted with additive noise denoted by B . In our simulations, we consider an objective with numerical aperture $NA = 1.5$ and $N = 24$ illuminations corresponding to incident plane waves with a fixed polar angle of 70° and azimuthal angles varying from 0 to 2π with $\pi/24$ steps. We assume that the intensity, recorded at \mathbf{r}_\parallel on the image plane, coming from a point source placed at $\mathbf{r}' = (\mathbf{r}'_\parallel, z')$ in the near vicinity of the grating is $P(\mathbf{r}_\parallel - \mathbf{r}') = |J_1(2\pi NA |\mathbf{r}_\parallel - \mathbf{r}'_\parallel|/\lambda)/(2\pi NA |\mathbf{r}_\parallel - \mathbf{r}'_\parallel|/\lambda)|^2$, where J_1 is the first-order Bessel function of the first kind. This crude approximation implies, in particular, that the emitted field does not depend on the position of the source on the grating. It is expected to be valid if the source emission wavelength is different from the wavelengths at which the grating is resonant.

Once the different images of the sample have been obtained for the $N = 24$ illuminations, we use a linear inversion scheme to reconstruct the fluorophore's density. More precisely, we define an investigation domain Ω above the grating, and we estimate the fluorophore density \tilde{O} at the nodes of a regular meshing of Ω to minimize the cost function

$$\mathcal{F}(\tilde{O}) = \sum_{l=1}^N \sum_{\mathbf{r} \in \Omega} \|I_l(\mathbf{r}) - (\tilde{O} \times E_l) \otimes P(\mathbf{r})\|^2. \quad (2)$$

A conjugate gradient algorithm is applied to solve this linear inverse problem [21]. Since we are dealing with surface imaging, the investigation domain Ω is a thin slice just above the grating that is regarded as a surface, and its transverse dimensions are taken equal to those of the recorded images.

To study numerically the transverse and axial resolution of GA-TIRFM, we consider a three-dimensional sample made of two layers of small fluo-

rescent beads. The first layer is deposited on the substrate, while the other floats at $z=50$ nm above the grating [see Fig. 2(a)]. We simulate the intensity recorded at the image plane of the microscope by accounting for the two layers of fluorophores in Eq. (1) and corrupting the data with a Gaussian random background noise with variance 0.05 of the maximum intensity [see Fig. 2(b)]. For comparison, we also simulate the SW-TIRFM experiment described in [16]. In this configuration, the sample is deposited on a conventional glass slide and is illuminated by a standing evanescent wave that is rotated about the vertical axis and translated three times to ensure a homogeneous illumination of the sample. We plot in Fig. 3 the reconstructed density of fluorophores obtained with the same linear inversion scheme for the two experiments. We observe that in the GA-TIRFM simulated experiment, Fig. 3(a), only the fluorophores lying on the grating are visible on the reconstructed image. In contrast, in the SW-TIRFM, the image is strongly perturbed by the signal emitted by the fluorophores above the substrate [Fig. 3(b)]. The shadow of the latter is clearly visible on the reconstruction. Moreover, as expected, the transverse resolution of the GA-TIRFM is improved by a factor of two compared with that of the SW-TIRFM. In particular, it is possible to distinguish two beads that are separated by $\lambda/10$ (i.e., half the period of the grating) in the GA-TIRFM setup.

This numerical study points out the clear improvement of both axial and transverse resolution that could be obtained with GA-TIRFM compared with SW-TIRFM. Moreover, GA-TIRFM can be implemented in a conventional total internal reflection fluorescence microscope since it does not require a complex interference setup as in the standing-wave technique. It suffices to replace the conventional support of the sample by a periodically nanostructured

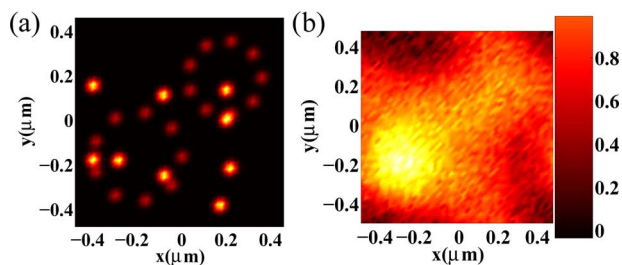


Fig. 2. (Color online) (a) Fluorophore density distribution of the sample in the (x, y) plane. The bright spots represent the beads deposited on the substrate, and the ghost spots represent the beads at $z=50$ nm above the substrate. (b) Simulated intensity obtained on the image plane of the microscope for the first illumination.

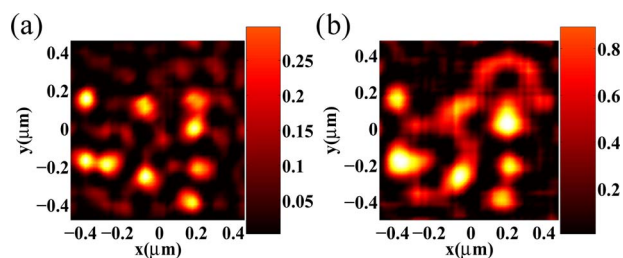


Fig. 3. (Color online) (a) Reconstructed density of fluorophores obtained with the linear inverse procedure from the 24 images in the GA-TIRFM. (b) Same as (a) in the SW-TIRFM configuration.

substrate, to record several images for different successive plane wave illuminations, and to use an inversion technique for reconstructing the fluorophore density. The image resolution is limited not by the wavelength of illumination but, essentially, by the period of the grating.

References

1. G. Cox and C. J. R. Sheppard, *Microsc. Res. Tech.* **63**, 18 (2004).
2. S. Hell, *Science* **25**, 1153 (2007).
3. M. Gustafsson, *Proc. Natl. Acad. Sci. USA* **102**, 13081 (2005).
4. S. Bretschneider, C. Eggeling, and S. W. Hell, *Phys. Rev. Lett.* **98**, 218103 (2007).
5. D. Marks and P. S. Carney, *Opt. Lett.* **30**, 1870 (2005).
6. J.-J. Greffet and R. Carminati, *Prog. Surf. Sci.* **56**, 133 (1997).
7. Z. Liu, H. Lee, L. Xiong, C. Sun, and X. Zhang, *Science* **315**, 1686 (2007).
8. I. I. Smolyaninov, Y. J. Hung, and C. C. Davis, *Science* **315**, 1699 (2007).
9. I. I. Smolyaninov, J. Elliott, A. V. Zayats, and C. C. Davis, *Phys. Rev. Lett.* **94**, 057401 (2005).
10. A. Sentenac, P. C. Chaumet, and K. Belkebir, *Phys. Rev. Lett.* **97**, 243901 (2006).
11. Z. Liu, S. Durant, H. Lee, Y. Pikus, N. Fang, Y. Xiong, C. Sun, and X. Zhang, *Nano Lett.* **7**, 403 (2007).
12. D. Toomre and D. J. Manstein, *Trends Cell Biol.* **11**, 298 (2001).
13. R. Heintzmann and C. Cremer, *Proc. SPIE* **3568**, 185 (1998).
14. M. Gustafsson, *J. Microsc.* **198**, 82 (2000).
15. J. Frohn, H. Knapp, and A. Stemmer, *Proc. Natl. Acad. Sci. USA* **97**, 7232 (2000).
16. E. Chung, D. Kim, and P. So, *Opt. Lett.* **31**, 945 (2006).
17. G. Cragg and P. So, *Opt. Lett.* **25**, 46 (2000).
18. R. Petit, *Electromagnetic Theory of Gratings* (Springer-Verlag, 1980).
19. E. N. Economou, *Phys. Rev.* **182**, 539 (1969).
20. L. Li, *J. Opt. Soc. Am. A* **14**, 2758 (1996).
21. P. C. Chaumet, K. Belkebir, and A. Sentenac, *Phys. Rev. B* **69**, 245405 (2004).